

The influence of wind and temperature gradients on sound propagation, calculated with the two-way wave equation

L. Nijs

Research Institute of Urban Planning and Architecture, Delft University of Technology, Berlageweg 1, 2628 CR, Delft, Netherlands

C. P. A. Wapenaar

Faculty of Applied Physics, Group of Seismics and Acoustics, Delft University of Technology, Delft, Netherlands

(Received 19 December 1988; accepted for publication 15 December 1989)

A method is introduced to calculate the influence of wind and temperature gradients in stratified media on sound propagating above an absorbing ground surface. It is based on the "two-way wave equation" for the Fourier transforms of the sound pressure P and its derivative V . The vector containing P and V is stepwise extrapolated through the medium in the direction perpendicular to the ground surface, fulfilling the boundary conditions at the ground surface, at a top level, and at the source height. The propagation equations for P and V appear as simple plane-wave equations, and computer (CPU) time within each layer is very low. Therefore, many thin layers (in the order of centimeters if desired) can be applied, and any complicated gradient can be used. Calculations for a homogeneous atmosphere, with a computer program based on this model, show an excellent agreement with previous models. When a wind profile is present, results are mainly compared with measurements by Parkin and Scholes [P. H. Parkin and W. E. Scholes, *J. Sound Vib.* **1**, 1–13 (1964); **2**, 353–374 (1964)]. They show very good agreement in the no-wind and downwind cases. In the upwind situation, agreement is very good below 500 Hz. Above this value the model does not predict sound to penetrate into the shadow region, while Parkin and Scholes found (low) sound levels.

PACS numbers: 43.28.Fp, 43.20.Fn

INTRODUCTION

A model to calculate the influence of wind and temperature gradients on sound propagation above a ground surface of finite impedance was developed about 10 years ago by de Jong,^{1,2} using extrapolation models originating from seismic research. The sound field is extrapolated step by step through a layered medium, and in every layer the influence of wind and temperature can be varied. The extrapolation is basically in the x direction (parallel to the ground surface), but to account for the absorption of the ground surface, steps in the z direction (perpendicular to the surface) are also required. Good agreement between the model and outdoor measurements was found in the frequency regions below 200 Hz and above 500 Hz. However, in the region between 200 and 500 Hz, discrepancies between the model and measurements were observed.

Subsequently, similar models have been published.^{3–6} All of the investigators in these publications used extrapolation techniques in layers and tried to solve the basic equations for sound propagation with Bessel–Hankel transforms in the Fourier domain. The computer model presented in this paper departs from the same origin. The solution of the "full wave equation" in the Fourier domain is written in matrix form as a "two-way wave equation," calculating upward and downward traveling waves simultaneously.⁷ The expression "two-way wave equation" might be a bit misleading; it originates from seismic models (see Ursin⁸ for an overview) to distinguish these propagation methods from

older techniques where only one-way traveling waves are considered.

The basic equations are written in the spatial Fourier domain, dividing the medium into horizontal layers. That means that the sound waves are decomposed into a set of plane waves. Each plane wave is described by the Fourier transform of the sound pressure and its derivative, which is proportional to the Fourier transform of the normal component of the particle velocity. The plane waves are subjected to the wave equation (which has become one dimensional because of the Fourier transform) for each layer, incorporating wind and temperature effects. When the propagation through all layers has been completed, an inverse Fourier transform is carried out to find the real sound pressure.

The strength of the present model is that the propagation equations for each plane wave within a layer are extremely simple. There is no need to calculate integrals and/or series.

Because of the simplicity of the propagation equations within each layer, the calculation time in a computer model is short, and therefore many thin layers (if desired, in the order of a few centimeters) can be introduced and a complicated gradient can be used. Previous models (using Bessel–Hankel transforms) must use comparatively large layers in order to keep the calculation time low.

The one physical restriction of our model is that it works only for stratified media. Because of computer time, two more restrictions are made.

(1) The theory is basically three dimensional; however, we restricted the model to two dimensions.

(2) Computer time tends to increase sharply with frequency. Therefore, we introduce a method which we call "zoom-fft." This leads to some small errors above the sound source, which is outside the region of interest.

Although our computer time is low when compared to other models, it still does not run on a personal computer (PC). Because of the vector nature of the plane waves, it is very well suited to run on a vector-based computer.

I. THEORY

A. The wave equation

There are two basic equations describing the acoustical behavior of a flowing medium. These are for the nonlinear equation of continuity and the nonlinear equation of motion. If we furthermore assume that the medium follows Hooke's law, they can be written as

$$\nabla \cdot \mathbf{v}_t + \frac{1}{K} \left(\frac{\partial}{\partial t} + \mathbf{v}_t \cdot \nabla \right) p_t = 0 \quad (1)$$

and

$$\nabla p_t + \rho_t \left(\frac{\partial}{\partial t} + \mathbf{v}_t \cdot \nabla \right) \mathbf{v}_t = \mathbf{0}, \quad (2)$$

with p_t the total pressure in the medium, \mathbf{v}_t the total particle velocity, ρ_t the total mass density, and K the compression modulus. In Eq. (2), the term giving the influence of gravity has been left out, which means that the barometric pressure must be constant with height.

The total pressure, velocity, and density are split into two parts:

$$p_t = P_0 + p, \quad (3a)$$

$$\rho_t = \rho_0 + \rho, \quad (3b)$$

$$\mathbf{v}_t = \mathbf{w} + \mathbf{v}, \quad (3c)$$

where P_0 , ρ_0 , and \mathbf{w} are time-invariant quantities, describing the mean pressure, density, and velocity of the flowing medium, and where p , ρ , and \mathbf{v} are the corresponding time-variant quantities, describing the acoustic-wave field. In the following, we assume the acoustical pressure and density to be small in comparison with the time-invariant quantities and the time-invariant quantities varying only slowly with space, and so

$$|p| \ll |P_0| \text{ and } |\nabla P_0| \ll |\nabla p|, \quad (4a)$$

and, similarly,

$$|\rho| \ll |\rho_0| \text{ and } |\nabla \rho_0| \ll |\nabla \rho|. \quad (4b)$$

By definition it is assumed that variables determining the medium (K , ρ_0 , and \mathbf{w}) depend only on the vertical coordinate z (the so-called stratified medium). In addition, we assume that the flow of the medium is in the x and y directions only, and so the z component of \mathbf{w} is equal to 0. Under these conditions, we find

$$\nabla \cdot \mathbf{w} = 0. \quad (4c)$$

Now, the linearized versions of Eqs. (1) and (2) read

$$\nabla \cdot \mathbf{v} + \frac{1}{K} \left(\frac{\partial}{\partial t} + \mathbf{w} \cdot \nabla \right) p = 0 \quad (5)$$

and

$$\nabla p + \rho_0 \left(\frac{\partial}{\partial t} + \mathbf{w} \cdot \nabla \right) \mathbf{v} + \rho_0 v_z \frac{\partial \mathbf{w}}{\partial z} = \mathbf{0}. \quad (6)$$

We now apply a threefold Fourier transform on these equations with $t \rightarrow \omega$, $x \rightarrow k_x$, and $y \rightarrow k_y$, defined for the pressure as

$$P(k_x, k_y, z, \omega) = \iiint_{-\infty}^{\infty} p(x, y, z, t) \times e^{-j\omega t} e^{jk_x x} e^{jk_y y} dt dx dy, \quad (7a)$$

and, for the backward transform,

$$p(x, y, z, t) = \frac{1}{8\pi^3} \iiint_{-\infty}^{\infty} P(k_x, k_y, z, \omega) \times e^{j\omega t} e^{-jk_x x} e^{-jk_y y} d\omega dk_x dk_y. \quad (7b)$$

A similar Fourier transform is used for the transform from \mathbf{v} to \mathbf{V} .

In many cases, k_x and k_y in Eqs. (7) are taken as real variables and the integration in Eq. (7b) is carried out along the real axis. However, the functions to be integrated may have poles on the real axis, and in that case k_x and k_y must be complex variables and a branch must be taken through the complex plane. We will come back to this problem in Sec. I E.

Now a new variable μ is introduced, defined as

$$\mu = 1 - w_x k_x / \omega - w_y k_y / \omega, \quad (8)$$

where w_x and w_y are the x and y components of \mathbf{w} .

Using Eqs. (7a) and (8), Eq. (5) is transformed to

$$\frac{\partial V_z}{\partial z} - jk_x V_x - jk_y V_y + \frac{j\omega}{K} \mu P = 0, \quad (9)$$

while Eq. (6) is written out in three equations:

$$-jk_x P + j\omega \rho_0 \mu V_x + \rho_0 \frac{\partial w_x}{\partial z} V_z = 0, \quad (10a)$$

$$-jk_y P + j\omega \rho_0 \mu V_y + \rho_0 \frac{\partial w_y}{\partial z} V_z = 0, \quad (10b)$$

$$\frac{\partial P}{\partial z} + j\omega \rho_0 \mu V_z = 0, \quad (10c)$$

where V_x , V_y , and V_z are the components of \mathbf{V} .

Now, the wavenumber k and two variables k_m and k_z are introduced, defined as

$$k^2 = \omega^2 \rho_0 / K, \quad (11a)$$

$$k_m = \mu k, \quad (11b)$$

$$k_z^2 = k_m^2 - k_x^2 - k_y^2. \quad (11c)$$

As K , μ , and ρ_0 may vary with z , k , k_m , and k_z also depend on z .

After eliminating \mathbf{V} from Eqs. (9) and (10), the following equation for P is found:

$$\rho_0 \mu^2 \frac{\partial}{\partial z} \left(\frac{1}{\rho_0 \mu^2} \frac{\partial P}{\partial z} \right) + k_z^2 P = 0. \quad (12)$$

B. The wave equation in air

Until now, only a few assumptions were made about the medium itself (satisfying Hooke's law; no shear, no influ-

ence of static pressure). Equation (12), for instance, can be applied in all kinds of media with varying values of μ , ρ_0 , and K . They are, for instance, used in seismic models if shear waves are absent and $\mu = 1$.

If used in air, a few common assumptions can be made. First, we assume air to be an ideal gas and the sound propagation to be an adiabatic process. In that case, $K = \gamma P_0$, where P_0 is the static pressure, and $\gamma = C_p/C_v$ (the ratio of the specific heats). With these assumptions, the variables k and k_m can be rewritten. If we introduce a variable c (representing the local sound speed when the wind speed is not taken into account) and the Mach vector \mathbf{m} (both depending on z), we find

$$c^2 = \gamma P_0 / \rho_0, \quad (13a)$$

$$m_x = w_x / c, \text{ and } m_y = w_y / c, \quad (13b)$$

$$k = \omega / c, \quad (13c)$$

$$k_m = \omega / c - m_x k_x - m_y k_y. \quad (13d)$$

In fact, c incorporates the effects of temperature while \mathbf{m} stands for the wind effect. In our derivation they are treated differently, because the first variable is a scalar and the second a vector.

With Eqs. (13), Eq. (12) can now be written in two ways:

$$\frac{\partial}{\partial z} \left(\frac{1}{k_m^2} \frac{\partial P}{\partial z} \right) + \frac{k_z^2}{k_m^2} P = 0, \quad (14)$$

or as

$$P'' - 2(k'_m/k_m)P' + k_z^2 P = 0, \quad (15)$$

where the primes denote the derivatives with respect to z .

The given derivation of the wave equation in air is not new. An equation very similar to Eq. (15) appeared previously in an article by Pridmore-Brown, written in 1962 [Eq. (7) in Ref. 9]. Pridmore-Brown includes the static pressure in the derivation of the wave equation. From that equation, it can be concluded that the gradient of the static pressure has only a very minor influence when compared with the wind gradients used in the remainder of this article. However, in a perfect stable atmosphere (no wind, a temperature gradient of -0.007 K/m and a pressure gradient of -12 Pa/m), the influence of the pressure gradient appears much greater than the influence of the temperature gradient. Therefore, care must be taken when omitting the static pressure.

The equations given here are three dimensional. Throughout the work presented in this paper, however, we confined ourselves to the two-dimensional case, mainly to save computer space and to avoid two-dimensional Fourier transforms. Until now we have never found any evidence that inaccuracies in our results are due to this restriction. This implies that Eqs. (13d) and (11c) become

$$k_m = \omega / c - m k_x, \quad (16a)$$

$$k_z^2 = k_m^2 - k_x^2, \quad (16b)$$

with $m_x = m$.

C. The wave equation in matrix form

Pridmore-Brown and other investigators (mentioned in the Introduction) tried to solve Eq. (15) with a Bessel-Hankel transform, after writing the equation in circular coordinates. At this point we take a new direction.

First, we introduce a source situated at $(0, z_s)$. It is possible to introduce the source term in Eqs. (1) and (2). Then, a "force" can be introduced by adding a term to the right-hand side of Eq. (2), while similarly a "volume injection" must be introduced in both Eqs. (1) and (2). They represent a dipole and a monopole source, respectively, where the monopole source stands acoustically for a piston in a long tube or an ideal loudspeaker. Since all previous investigators used monopole sources (for calculations and for measurements), we also restrict ourselves to this source type, and so the force is left out, and only the volume injection is taken into account.

Introducing the monopole source, Eq. (14) can be written in matrix form as

$$\frac{\partial}{\partial z} \begin{bmatrix} P \\ U \end{bmatrix} = \begin{bmatrix} 0 & k_m^2 \\ -k_z^2 & 0 \end{bmatrix} \begin{bmatrix} P \\ U \end{bmatrix} + \begin{bmatrix} 0 \\ S(\omega)\delta(z-z_s) \end{bmatrix}, \quad (17)$$

with

$$U = \frac{1}{k_m^2} \frac{\partial P}{\partial z}. \quad (18)$$

U is proportional to V_z ; the multiplication factor is equal to $j\omega\mu/\gamma P_0$. The rightmost term represents the source vector for a monopole source. If a dipole is also used, it will appear as a delta function in the upper part of this vector. The source strength $S(\omega)$ is rather arbitrary; we will come back to this subject in Sec. I D.

Introducing a new notation for the vectors and the matrix, Eq. (17) yields

$$\frac{\partial}{\partial z} \mathbf{Q}(z) = [A(z)]\mathbf{Q}(z) + \mathbf{S}(z). \quad (19)$$

Departing from a plane $z = z_0$ and extrapolating to a certain z plane, the solution of Eq. (19) can be written as (see, for instance, Ref. 10)

$$\mathbf{Q}(z) = [W(z, z_0)]\mathbf{Q}(z_0) + \int_{z_0}^z [W(z, \zeta)]\mathbf{S}(\zeta)d\zeta, \quad (20)$$

where the matrix $[W]$ has to satisfy the differential equation

$$\frac{\partial}{\partial z} [W(z, z_0)] = [A(z)][W(z, z_0)]. \quad (21)$$

The solution of Eq. (21) will be given below; we start rewriting Eq. (20):

$$\mathbf{Q}(z) = [W(z, z_0)]\mathbf{Q}(z_0), \quad z_s < z_0 \text{ or } z_s > z, \quad (22a)$$

$$\mathbf{Q}(z) = [W(z, z_0)]\mathbf{Q}(z_0) + [W(z, z_s)]\mathbf{S}_0, \quad z_0 < z_s < z, \quad (22b)$$

with

$$\mathbf{S}_0 = \begin{bmatrix} 0 \\ S(\omega) \end{bmatrix}. \quad (23)$$

The values of z in Eqs. (22a) and (22b) are given under the

assumption that $z > z_0$. For the opposite case, the boundaries must be interchanged.

Equation (22a) makes it possible to move stepwise through a medium. We find, for instance, the following two cases:

$$[W(z, z_0)] = [W(z, z_n)] \cdots [W(z_2, z_1)] [W(z_1, z_0)], \quad (24a)$$

$$[W(z, z_0)] = [W(z, z_s)] [W(z_s, z_0)]. \quad (24b)$$

With the use of Eq. (24b), Eq. (22b) can be written as

$$\mathbf{Q}(z) = [W(z, z_s)] [W(z_s, z_0)] \mathbf{Q}(z_0) + [W(z, z_s)] \mathbf{S}_0. \quad (25)$$

The differential equation (21) can only be solved if $[A(z)]$ is a simple function over the layer (which is not necessarily small). To avoid complicated solutions, the medium is often represented by small layers, each having a simple form of $[A(z)]$, but different for each layer. In that case, $[W]$ will also be different for each layer. Extrapolation is then carried out by a repeated application of Eq. (22a).

The solution of Eq. (21) is as follows. If $[A(z)] = [A]$ is not a function of z (that means that k_m has a constant value over the extrapolation layer), the solution can be easily found (see again Ref. 10):

$$[W(z, z_0)] = \exp\{[A](z - z_0)\}, \quad (26)$$

where the definition of the exponent can be given similar to the scalar definition:

$$\begin{aligned} \exp([B]) &= [E] + [B] + \frac{[B][B]}{2!} \\ &+ \frac{[B][B][B]}{3!} + \cdots, \end{aligned} \quad (27)$$

with $[E]$ the diagonal matrix having the values 1 on the diagonal.

Wapenaar⁷ gives a solution of Eq. (21) for a linear wind or temperature profile over a layer, when

$$k_m^2(z) = k_m^2(z_0)[1 + \kappa(z - z_0)], \quad (28)$$

with $|\kappa(z - z_0)| \ll 1$.

The first solution is used when the profile is divided in homogeneous layers, where Wapenaar's solution stands for linear layers (Fig. 1). We inserted both solutions in our computer program, but we did not find significant differences for the small layers we use. Because the second solution requires much more time and space in the computer, we decided to confine ourselves in the rest of this paper to Eq. (26).

To solve Eq. (26), the matrix $[A]$ can be decomposed with its eigenvectors:

$$[A] = [L][\Lambda][L^{-1}], \quad (29)$$

where $[\Lambda]$ is the diagonal matrix having the eigenvalues on the diagonal. By applying Eq. (27), it can be verified that

$$\begin{aligned} \exp([A]) &= \exp([L][\Lambda][L^{-1}]) \\ &= [L]\exp([\Lambda])[L^{-1}]. \end{aligned} \quad (30)$$

Now, introducing $\Delta z = z - z_0$, Eq. (26) can be rearranged to

$$[W(z_0 + \Delta z, z_0)] = [L]\exp([\Lambda]\Delta z)[L^{-1}]. \quad (31)$$

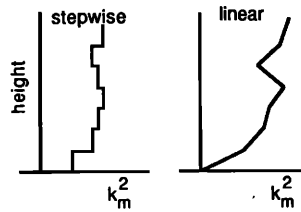


FIG. 1. The atmosphere can be given as stepwise layers or as layers with a linear profile.

In our case, the decomposition of the matrix $[A]$ is found as

$$[L] = \begin{bmatrix} 1 & 1 \\ -jk_z/k_m^2 & jk_z/k_m^2 \end{bmatrix}, \quad (32a)$$

$$[L^{-1}] = \frac{1}{2} \begin{bmatrix} 1 & -k_m^2/jk_z \\ 1 & k_m^2/jk_z \end{bmatrix}, \quad (32b)$$

$$[\Lambda] = \begin{bmatrix} -jk_z & 0 \\ 0 & jk_z \end{bmatrix}, \quad (32c)$$

and thus

$$\begin{aligned} [W(z_0 + \Delta z, z_0)] &= \frac{1}{2} \begin{bmatrix} e^{jk_z \Delta z} + e^{-jk_z \Delta z} & \frac{k_m^2}{jk_z} (e^{jk_z \Delta z} - e^{-jk_z \Delta z}) \\ \frac{jk_z}{k_m^2} (e^{jk_z \Delta z} - e^{-jk_z \Delta z}) & e^{jk_z \Delta z} + e^{-jk_z \Delta z} \end{bmatrix}. \end{aligned} \quad (33)$$

$[W]$ is the basic equation for the propagation through the medium, and, as can be seen, the entries within $[W]$ are very simple as only traveling and evanescent plane waves are found.

In many practical cases, k_x , k_m , and Δz are considered to be real variables. So, according to Eq. (16b), k_z is either real ($|k_x| < |k_m|$) or completely imaginary (the evanescent field where $|k_x| > |k_m|$). In that case, the entries in $[W]$ can be written as real cos, sin, cosh, and sinh functions. However, for reasons explained in the next section, we use Eq. (33) in the computer program in the complex form presented.

One remark about $[L]$ and $[L^{-1}]$ must be made: They give the coupling between two-way traveling waves and one-way pressure waves⁷:

$$\mathbf{P}(z) = [L^{-1}]\mathbf{Q}(z), \quad (34a)$$

$$\mathbf{Q}(z) = [L]\mathbf{P}(z), \quad (34b)$$

where \mathbf{P} is written as

$$\mathbf{P} = \begin{bmatrix} P^+ \\ P^- \end{bmatrix}, \quad (34c)$$

with P^+ and P^- the pressure waves traveling up and down, respectively. Equations (34) can be used to calculate the boundary conditions at the ground surface, because

$$P^+ = R_p P^-, \quad (35)$$

with R_p the plane-wave reflection coefficient.

D. The extrapolation model

A computer model was developed on the basis of a stepwise extrapolation through the medium. The extrapolation

starts at a certain height (the top level, for instance, $z = 50$ m), where P and U are calculated assuming that, above this level, only upgoing waves are present. Making use of Eqs. (32a) and (34b), the starting vector then becomes

$$\mathbf{Q}_t = \begin{bmatrix} P(z_t) \\ U(z_t) \end{bmatrix} = \begin{bmatrix} 1 & 1 \\ -jk_z/k_m^2 & jk_z/k_m^2 \end{bmatrix} \begin{bmatrix} P^+(z_t) \\ 0 \end{bmatrix} = \begin{bmatrix} 1 \\ -jk_z/k_m^2 \end{bmatrix} P^+(z_t). \quad (36)$$

At this stage in the calculations, only the ratio of P and U is important, and so for the moment $P^+(z_t)$ is given the value 1. The extrapolation is carried out from the starting plane to the source plane in given steps (see, also, Sec. II A), where the resulting P_u and U_u are calculated. The subscript u refers to the upper half-space.

A restart is made at the ground level, where $P^+ = R_p P^-$. Therefore, here we find

$$\mathbf{Q}_g = \begin{bmatrix} P(z_g) \\ U(z_g) \end{bmatrix} = \begin{bmatrix} 1 & 1 \\ -jk_z/k_m^2 & jk_z/k_m^2 \end{bmatrix} \begin{bmatrix} R_p P^-(z_g) \\ P^-(z_g) \end{bmatrix} = \begin{bmatrix} R_p + 1 \\ -jk_z/k_m^2 (R_p - 1) \end{bmatrix} P^-(z_g). \quad (37)$$

Again, we choose $P^-(z_g) = 1$. For R_p , we use the equation for the locally reacting case:

$$R_p = \frac{Z \cos \varphi - 1}{Z \cos \varphi + 1} = \frac{Zk_z/k_m - 1}{Zk_z/k_m + 1}, \quad (38a)$$

where φ gives the angle of incidence of the plane wave at the ground surface and Z is the specific acoustic impedance as given by the well-known equations introduced by Delany and Bazley¹¹:

$$\text{Re}(Z) = 1 + 0.051(2\pi\sigma/\omega)^{0.75}, \quad (38b)$$

$$\text{Im}(Z) = -0.0769(2\pi\sigma/\omega)^{0.73}, \quad (38c)$$

where σ is the estimated flow resistance of the ground surface (in N s m^{-4}), while all the other variables are taken at ground level, which also implies that there is no wind speed. The sign of $\text{Im}(Z)$ is taken to be negative, because in our conventions a pressure wave traveling in the positive z direction has a negative exponent. Delany and Bazley also used these conventions in their original paper, but many investigators use positive signs for $\text{Im}(Z)$ and the exponent.

From the ground level, extrapolation is carried out up to the source level, where P_l and U_l are calculated, the index l denoting values for the lower half-space.

The given calculation of the starting vectors with Eqs. (36) and (37) is only one way to describe the problem. Another way is to calculate the specific acoustic impedances at the top and ground level, which can easily be done because U is proportional to V_z and hence P/U is proportional to the specific impedance. It is obvious that the result remains the same.

The next step in our model is to calculate the sound pressure at the source level. From Eqs. (22b) and (23) (where z and z_0 both tend to z_s), it can be seen that P for the lower and the upper half-space must be the same; we call this value P_s . From the same equations, we find

$$U_{su} = U_{sl} + S(\omega), \quad (39)$$

where U_{su} and U_{sl} are the values of U for the upper and lower half-space. Since the ratios of P and U are known for both half-spaces, the values of U_{su} and U_{sl} can be eliminated, and P_s can be written as

$$P_s = [(P_u P_l)/(P_l U_u - P_u U_l)] S(\omega). \quad (40)$$

At this stage, $S(\omega)$ must also be chosen. In a homogeneous atmosphere without ground surface, P_s can be calculated from Eqs. (36), (37) (with $R_p = 0$), (33), and (40) as

$$P_s = (-k_0^2/2jk_z) S(\omega), \quad (41)$$

with k_0 the value of ω/c when there is no wind or temperature profile. For this particular case, the Fourier transform can be found in closed form. For instance, using Berkhout's calculation¹² and leaving out the Hankel function for the nearfield, we find in two dimensions:

$$P = (jk_z)^{-1} e^{-jk_z|z-z_l|} \Leftrightarrow p(x,z,\omega) = (2\pi k_0 r)^{-1/2} e^{-j(k_0 r + \pi/4)}, \quad (42)$$

where r is the distance between source and receiver.

Now, the value of $S(\omega)$ will be found also as a multiplication factor in the x,z domain. We decided to use the following values for two cases.

(1) In case 1 (Figs. 3–5), we very arbitrarily gave $S(\omega)$ the value 2. Thus the 0-dB level in the figures for the k_x domain is found. In the x,z domain, a multiplication factor $k_0^{3/2}(2\pi)^{-1/2}$ is found from Eqs. (41) and (42), which defines the 0-dB level.

(2) In the following frequency plots (Figs. 6–11), the values in the x,z domain are compared with free-field propagation for the same values of x and z and thus of r . Again, we took $S(\omega) = 2$, but, for every microphone position, a multiplication with $(2\pi r)^{1/2} k_0^{-3/2}$ is also used in the x,z domain.

E. Avoiding poles of the monopole source

The value of P in Eq. (42) has a pole when $|k_z| = 0$, which is for waves traveling in the x direction. These waves are the most important, and so a solution for this problem has to be found.

When a ground plane is present and the atmosphere is inhomogeneous, P has a more complicated form, but in any case it has a sharp peak. Applying a standard backward complex fast Fourier transform (CFFT⁻¹) from a computer library leads to errors in the x domain. The solution for this problem is the application of a complex value k_x by writing

$$k_x = k_r + jk_i, \quad (43)$$

where k_r and k_i are real variables. The result of this method is that the amplitude of the pressure P still has a finite value when $k_r = k_0$. This method is commonly used in seismic models and may lead to rather complicated integration methods. However, in our case we were able to simplify the problem by using the integration path given in Fig. 2.

The path is given for positive values of k_r . A similar path should be taken for negative values, but, as we calculated the integral for positive values only (as explained in the next section), the negative path of the integral can be left out.

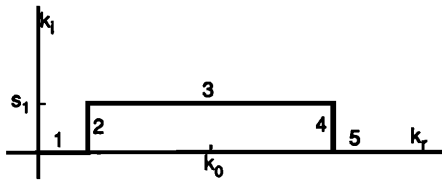


FIG. 2. The integration path for the calculation of the Fourier transform.

The Fourier transform can be written as

$$p(x, z, \omega) = \frac{1}{2\pi} \int_{k_i} P(k_x, z, \omega) e^{-jk_r x} dk_x. \quad (44)$$

Because the important values of $|P|$ are around k_0 , the contributions of the integration paths 1, 2, 4, and 5 can be neglected. Then [making use of Eq. (43) with a constant value s_1 for k_i], Eq. (44) can be written as

$$\begin{aligned} p(x, z, \omega) &\approx \frac{\exp(s_1 x)}{2\pi} \int_{-\infty}^{\infty} P(k_x, z, \omega) e^{-jk_r x} dk_x \\ &= \exp(s_1 x) \text{CFFT}^{-1}, \end{aligned} \quad (45)$$

and now a standard computer library routine can be used to carry out the Fourier transform.

Calculations for the homogeneous case prove that the method is very effective when s_1 is on the order of the step in k_r (we use $s_1 = k_{\text{Nyq}}/N$, coming back to k_{Nyq} and N in Sec. II B). The only disadvantage of the method given here is that the values of k_x , k_m , etc., are complex and require double space in the computer, and extra time is needed for calculations with complex numbers instead of real variables.

II. THE COMPUTER PROGRAM

A. The value of the extrapolation interval

Before the extrapolation program is started, the z levels (microphone levels) must be given where the sound pressure has to be calculated. During all the calculations presented here, we used 32 z planes ranging from ground level to 12.4 m in steps of 0.4 m. This last value may differ from the extrapolation step chosen, because the extrapolation step is related to the wavelength of the sound. For frequencies above 500 Hz, the extrapolation step becomes smaller than 0.4 m (see Sec. II B). Because turning planes may occur above the value of 12.4 m, we started at $z = 50$ m. This last value is very high and could easily be chosen lower, especially at lower wind speeds. We made no attempt, however, to optimize the value of the top level.

There are two methods to calculate the sound pressure at the given z levels.

(1) Extrapolation takes place from both starting planes ($z = 50$ m and 0) toward the source level (z_s), where P_s is calculated with Eq. (40). From P_s , starting values are calculated for the values U_{sl} and U_{su} of both half-planes, and another set of extrapolations in the opposite direction is carried out toward the desired z levels. There, a CFFT^{-1} is carried out to transform to $p(x, z, \omega)$, and these values are stored in a file.

(2) During extrapolation from the starting planes to the source level, the values of $P(k_x, z, \omega)$ are stored in files when

the given z levels are crossed. Arriving at the source height, P_s and two correction coefficients A_u and A_l are calculated from P_s , P_u , and P_l for the upper and the lower half-space. At each z level, the pressure P is regained from the file, multiplied by A_u or A_l , and Fourier transformed. The value of $p(x, z, \omega)$ is stored in computer memory.

The second method requires more computer space and computer time, because there is more file handling. However, in the computer configuration we used, we ran into accuracy problems applying the first method. The evanescent field is calculated as a small difference of two very big numbers and, to get accurate results, a double-precision method is required (which was not available in our computer configuration) or special filtering techniques must be applied. For these reasons, we chose the second method.

When extrapolating, the amplitudes of P and U can be very large in the evanescent field. To avoid these problems, a few precautions were made.

(1) Only small steps can be made. We took $|\Delta z| = \lambda/2$, λ being the wavelength.

(2) When extrapolating in the region from 50–12.4 m, only the ratio of P and U is important, which is much smaller than P and U .

(3) In the region between ground level and 12.4 m, the values of P and U are multiplied by $\exp(jk_{z_0} \Delta z)$ after each extrapolation step, where k_{z_0} is constant with respect to z and is calculated as

$$k_{z_0} = (k_s^2 - k_x^2)^{1/2}, \quad (46)$$

with $k_s = \omega/c_s$, and c_s is the sound velocity at the source height. Before the Fourier transform at level z is carried out, P is multiplied by $\exp(-jk_{z_0} |z - z_s|)$.

Another criterion for the maximum step in the z direction is the steepness of the wind or temperature profile. We used the step of $\lambda/2$ in the region between 50 and 12.4 m. This value appeared satisfactory (even at a frequency of 50 Hz) because profile gradients are very small in that region.

Wind profiles can be very steep close to the ground. Therefore, a step of 5 cm is chosen in the region between 0 and 20 cm. In the region from 0.2 to 12.4 m, the step is taken as the smaller value of either $\lambda/2$ or 0.4 m.

The values of the steps are deduced by trial and error, and are found to give good results. It should be noted that not much effort was given to optimizing these values to speed up the computer program. It should be possible to find values of the step size that give quicker results.

B. Filtering, zooming, and the number of data points

In most computer models, the value of k_x is taken as a real value from $-k_{\text{Nyq}}$ to $+k_{\text{Nyq}}$. Assuming a positive value of the Mach value m , the negative and positive values of k_x may be considered as representing upwind and downwind, respectively. Because we had to be very careful with computer space, we decided to restrict ourselves to positive values of k_x only. To calculate the wave propagation from the source in the z direction (therefore, right above the source), positive and negative values around $k_x = 0$ are required. Thus, our choice of positive k_x numbers leads to small errors in the vicinity of the source. However, that re-

gion is not of very great interest to our problem. For the upwind case, a separate run with a negative value of m had to be carried out.

Wind and temperature effects occur at horizontal distances of 50 m and more from the source. On the other hand, we were interested in values of z below 12.4 m only; or, expressed as an angle, all effects occur within an aperture angle between zero and about 15 deg as seen from the source. Translated to the k_x domain, all interesting effects occur in a small band around $k_x = k_0$. This allows us to use narrow filters in the k_x domain, as (again) errors will be found only for the region above the source. An important consequence of this filtering technique is that the sample density in the region around $k_x = k_0$ can be enlarged by using a smaller value of Δk_x . We call this method our "zoom-fft," which has as an advantage that longer distances in the x domain can be produced while keeping the total number of k_x values constant. A small disadvantage (apart from inaccuracies close to the source) is that computational noise may occur from aliasing at very low pressure levels, which is the case in the upwind shadow regions at high frequencies.

The method developed in this paper is very well suited for running on a vector machine, because all values of k_x , k_m , k_z , P , and U can be considered as complex vectors. We used a simple HP-1000 computer in conjunction with an FPS-array processor that is able to contain 64K real numbers. This means that, in our program structure, where the vectors are simultaneously in the memory of the array processor, the maximum number of vector elements is 4096 (complex values). Before Fourier transforming, a few vectors are scratched and the number of complex data points is enlarged to 8192 by adding zeros.

We choose a value of 400 m as the Nyquist value in the x domain for each frequency we ran on the computer, and 21 frequencies were chosen in $\frac{1}{2}$ -octave values, ranging from 50–4000 Hz. For k_{Nyq} , we find the value

$$k_{\text{Nyq}} = \pi N / x_{\text{Nyq}}, \quad (47)$$

from which we deduce

$$k_{\text{Nyq}} / k_0 = N c_0 / 2 x_{\text{Nyq}} f, \quad (48)$$

where f is the frequency and N is the number of data points. Choosing $f = 500$ Hz, $c_0 = 340$ m/s, and $N = 2048$ leads, for instance, to $k_{\text{Nyq}} / k_0 = 1.7408$, which is very well suited for our purpose. We decided to keep this value 1.7408 constant throughout all of our calculations and to select a combination of N and the zoom factor so as to have the Nyquist distance equal to 400 m. The values of Table I for the number of data points and the zoom factor for each frequency are chosen in the computer program.

A Nyquist distance of 400 m means that the wrap-around effect occurs every 800 m. With the type of filtering we use, aliasing occurs in the region from 700–800 m. The number of data points and number of steps increase with increasing frequency. Thus the calculation time depends strongly on the frequency. To complete 32 z levels with x ranging from 0–800 m requires about 45 s at 50 Hz. At 1000 Hz, CPU time is about 3 min, 50 s. At higher frequencies, we are able to keep the number of steps constant because of the zooming method chosen. That is why the CPU time remains 3 min, 50

TABLE I. The number of data points of the Fourier series (N) and the zoom factor as a function of the frequency to find a Nyquist distance of 400 m.

Frequency	N	Zoom factor
50	256	0.8
63	256	1.008
80	256	1.28
100	256	1.6
125	512	1.0
160	512	1.28
200	512	1.6
250	1024	1.0
315	1024	1.26
400	1024	1.6
500	2048	1.0
630	2048	1.26
800	2048	1.6
1000	4096	1.0
1250	4096	1.25
1600	4096	1.6
2000	4096	2.0
2500	4096	2.5
3150	4096	3.15
4000	4096	4.0

s for higher frequencies.

After each monochromatic run, we select 10 distances at 10 z levels to save in computer memory. After a complete run, we have 21 frequencies by 10 distances by 10 z levels. It takes about 70 min to complete such a run.

III. RESULTS

A. The wind and temperature profile used

There are only limited data available on the wind profile in the lower layers of the atmosphere, especially in the first few meters above the ground. We therefore made some assumptions. We decided to model the wind speed with the familiar power law and assumed that it is also valid at the ground surface (which is not strictly the case):

$$w(z) = w_{10}(z/10)^\alpha, \quad (49)$$

where w_{10} is the wind velocity at 10 m high, and α depends on the surface roughness. When $\alpha = 1$, we find a linear wind profile. The log profile, which is preferred in most meteorological publications, cannot be used, because it has no meaning close to the ground.

For the temperature profile, more data are available. We used, for instance, profiles as measured by Huisman *et al.*¹³ and Geiger.¹⁴ From the results of Geiger, we deduced an exponential temperature profile.

In theory, because the temperature effect is a scalar and the wind effect is a vector, there is a difference between the effects of wind and temperature profiles. Dividing Eq. (16a) into two separate parts for the temperature and wind profiles, respectively, we find

$$k_m(z) = \omega/c(z), \quad (50a)$$

$$k_x(z) = k_0 - m(z)k_x. \quad (50b)$$

Now, $c(z)$ can be written in terms of the temperature:

$$c(z) = c_0 [T(z)/T_0]^{1/2}, \quad (51)$$

where the indexes 0 denote the values at ground level.

Because the variations in the temperature are always small compared with T_0 , we find

$$k_m(z) \approx k_0 [1 - \Delta T(z)/2T_0], \quad (52)$$

with $\Delta T(z) = T(z) - T_0$.

As stated earlier, all of the important phenomena appear around $k_x = k_0$. If we had written k_0 instead of k_x in Eq. (50b), we would have found the same effects for the wind and temperature profiles. As an example, we find that the effects of a linear temperature profile of $0.86^\circ\text{C}/\text{m}$ correspond to a linear wind profile of 5 m/s at 10 m . In fact, calculations with the extrapolation model show that there are differences between a wind profile and a corresponding temperature profile, but they are small. For this reason we restrict ourselves to the wind profile (the vector approach) throughout the remainder of this paper.

B. An example of the computational flow

Figure 3(a) shows three examples of $|P(k_x, z, \omega)|$ at a receiver height of 1.6 m as a function of k_x , ranging from 0 to k_{Nyq} . The source height is 1.8 m , the frequency is 250 Hz ($k_0 = 4.62$), and, according to Eq. (47) and (48), k_{Nyq}

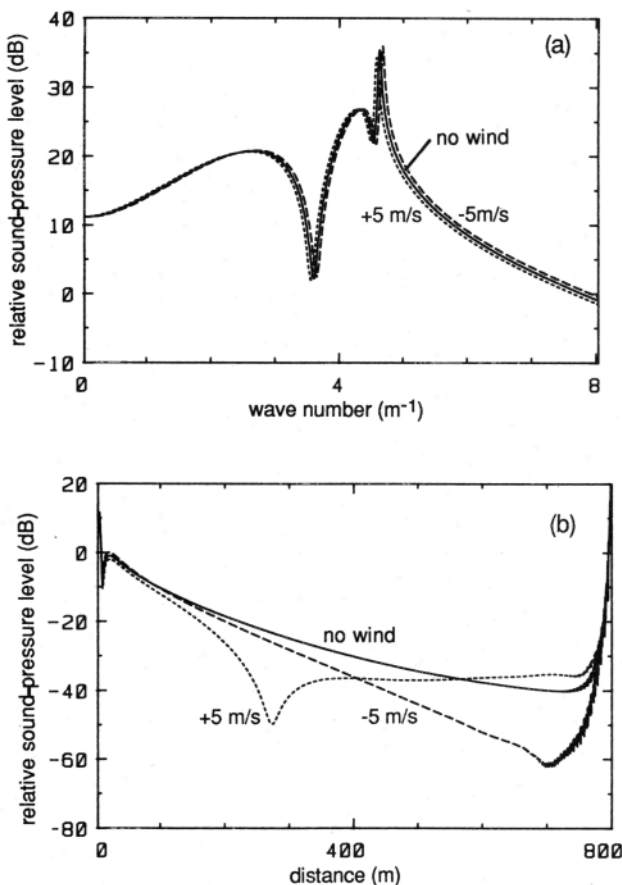


FIG. 3. (a) The sound-pressure level as a function of k_x for three different wind speeds and (b) after Fourier transforming to the x domain. Frequency is 250 Hz , source height is 1.8 m , receiver height is 1.6 m , $\sigma = 2 \times 10^5\text{ N s m}^{-4}$, and $\alpha = 0.14$.

$= 8.04$. In order to show more detail, the vertical axes are given as $20 \log(|P|)$, where the reference level was already given in Sec. II B. The oscillations are due to the interaction of direct waves and waves reflected at the ground surface. The flow resistance of the ground surface is taken as $\sigma = 2 \times 10^5\text{ N s m}^{-4}$.

Figure 3 shows that all important variations in amplitude between the homogeneous case and the cases with wind occur in the region where $k_x = k_0$, mainly because the curve is shifted to higher (upwind) or lower (downwind) values of k_x .

After filtering and a CFFT^{-1} , we find Fig. 3(b), which gives the value of $20 \log(|p(x, z, \omega)|)$ as a function of distance. Now, the x values range from 0 – 800 m , being twice the Nyquist distance. The figure shows wraparound effects in the region between 700 and 800 m . Doubling the number of data points proves that no aliasing occurs in the region up to about 700 m . However, for safety, we restrict ourselves to 400 m in the remainder of this paper. The downwind case shows a curve that is no longer monotonically decreasing. This effect was reported before by de Jong² and Raspet *et al.*³

Figure 3 gives the values at one z plane (1.6 m), but a complete computer run leads to a set of values of $20 \log(|p|)$, in $32\text{ }z$ planes from 0 to 12.4 m . From these values an isobar plot can be constructed, giving the curves with a constant value of the relative sound-pressure level in the x – z plane. Figure 4(a)–(c) gives the wind-free case, the downwind case, and the upwind case, respectively, now ranging from the source to a distance of 400 m . The dip found in Fig. 3(b) is, of course, found again in Fig. 4(b).

We note that, at the frequency taken here, the relative sound-pressure level with wind lies below the level for the homogeneous case. This effect is found in the region from 200 – 500 Hz . Outside this frequency region, the sound-pressure level mainly increases with increasing wind speed.

The dips as found in Figs. 3(b) and 4(b) can be very deep. Figure 5 shows three curves for wind speeds of 4 , 5 , and 6 m/s . The dip at 5 m/s at 200 m is the most extreme case we could find by trial and error. It shows nearly total extinction. This is probably due to the amplitude of the direct wave from source to receiver, as ray theory also predicts that the direct ray tends to *decrease* in a downwind situation. The dip changes rapidly if the wind speed differs only slightly. Therefore, it will be almost impossible to find these dips experimentally because there is always some variation in the wind speed that will tend to smear the dip. We simulated this effect by calculating an energy mean value over the three wind speeds. It is given as a solid line in the figure. The dips appear very sensitive to the shape of the wind profile. The calculations shown here are taken with a 0.14 exponent in the wind profile. When a linear profile is used, the dips are much less pronounced, although they never vanish completely.

C. The shape of the wind profile

All remaining figures in this paper are frequency plots. These plots are calculated at $\frac{1}{3}$ -octave intervals. In fact, these intervals are rather coarse, and the sharp dips, due to path length differences between direct and reflected sound that

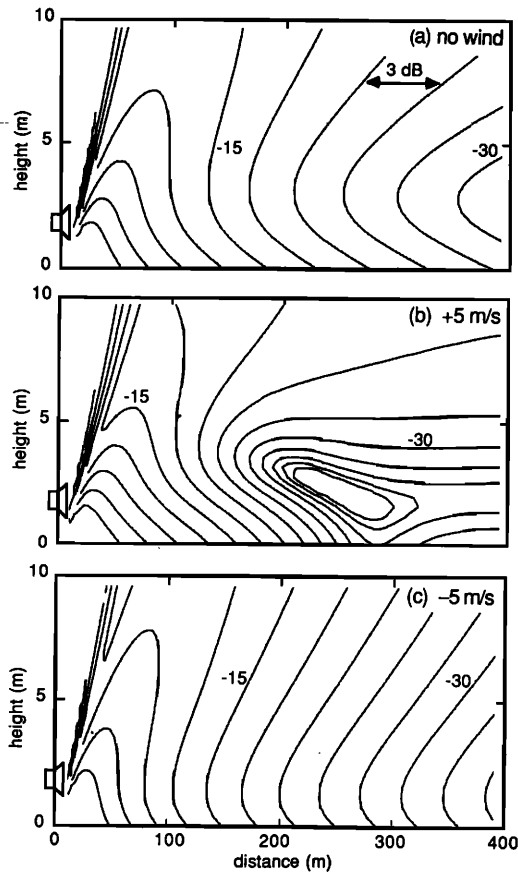


FIG. 4. Isobar plots calculated from the sound pressures at different z levels. Data as in Fig. 3.

occur at higher frequencies (above 1000 Hz), will not be accurately reproduced. In order to calculate these dips accurately, a smaller interval should be chosen.

The results appear very sensitive to the shape of the wind profile. To illustrate this effect, we calculated three frequency plots with three different profiles, as sketched in Fig. 6(a).

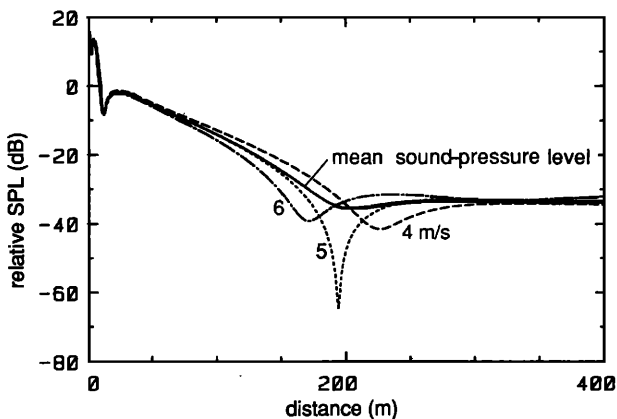


FIG. 5. Sound pressure as a function of x to illustrate dips. Frequency is 315 Hz, source height is 1.8 m, microphone height is 1.5 m, $\sigma = 25 \times 10^4 \text{ N s m}^{-4}$, and $\alpha = 0.14$.

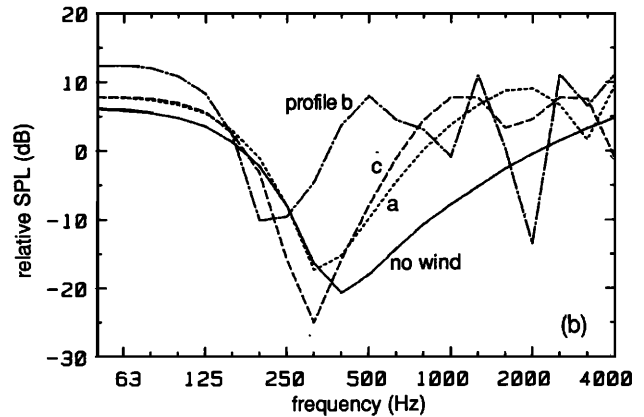
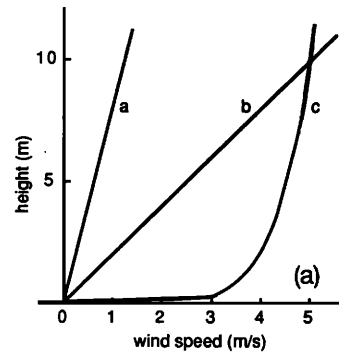


FIG. 6. (a) Three wind profiles: a, linear profile with wind speed 1.2 m/s at 10 m; b, linear with 5 m/s at 10 m; and c, $\alpha = 0.14$ and 5 m/s at 10 m; and (b) the frequency plots calculated with these profiles. Source height is 1.8 m, microphone height is 1.6 m, and source-receiver distance is 200 m, $\sigma = 2 \times 10^5 \text{ N s m}^{-4}$.

When z is higher than about 0.5 m, the linear curve with a wind speed of 1.2 m/s at 10 m has about the same gradient as the standard wind profile (5 m/s and $\alpha = 0.14$) used for most of our calculations. The other profile has the same wind speed at 10 m, but the gradient is totally different. As can be seen by comparing the curves labeled a and c with the curve for profile b in Fig. 6(b), the gradient appears much more important than the wind speed at 10 m.

It can be concluded that models that assume a linear wind profile could give satisfactory results as long as a good estimate is made of the wind gradient. The wind speed at a height of 10 m is not a good indicator of the profile. The use of this value in a linear profile will lead to a strong overestimation of the influence of the wind on sound propagation. Measuring results should always be accompanied by wind-speed measurements at different heights.

Throughout the rest of this paper, wind profile c in Fig. 6(a) is used with $\alpha = 0.14$. We want to compare our calculations with the measurements of Parkin and Scholes (Sec. III E), and this profile is most likely on the airfield where they took their measurements.

D. Wind speed and ground absorption

Figure 7 gives some results of the calculation with the model. The vertical scale is the sound-pressure level relative

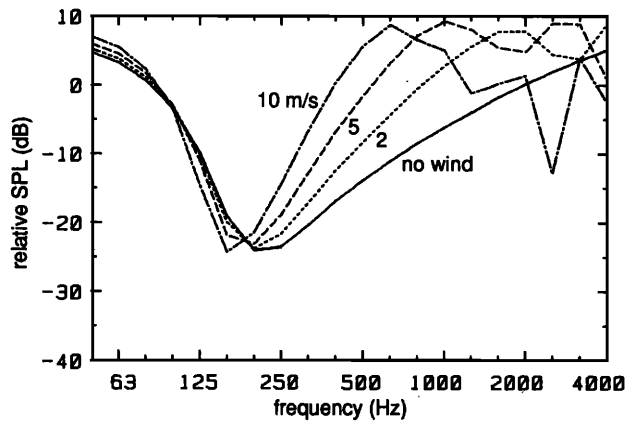


FIG. 10. As in Fig. 7, but with a more absorbing ground plane, $\sigma = 5 \times 10^4 \text{ N s m}^{-4}$.

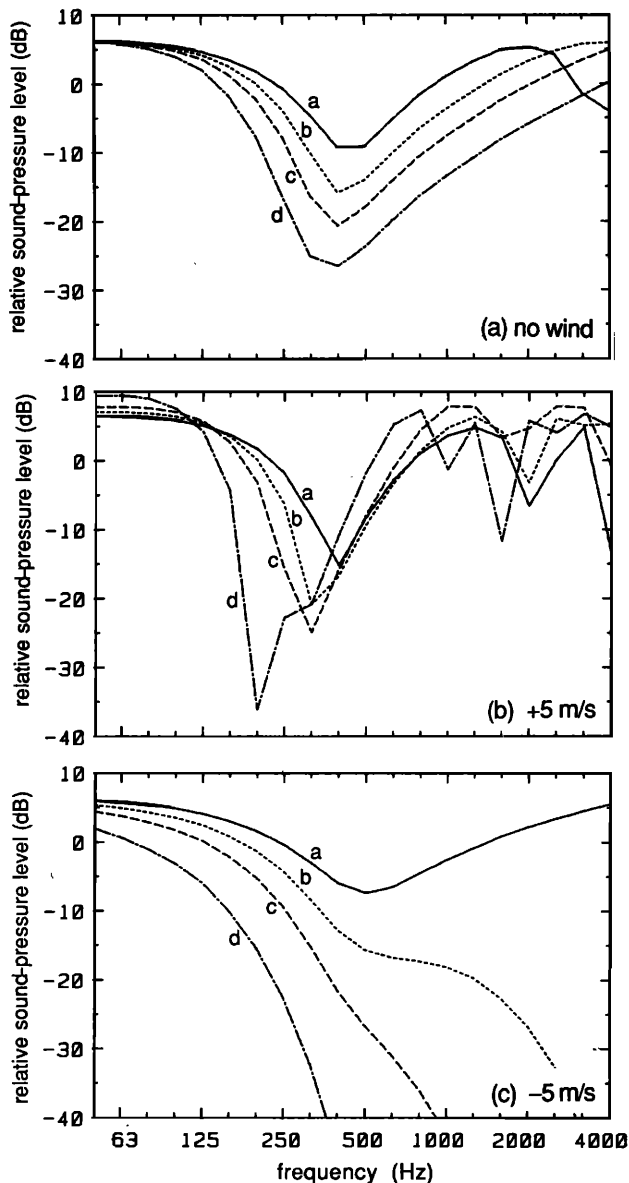


FIG. 11. Frequency plots with the source-receiver distance as the parameter. Sound level is compared to free-field propagation. Source height is 1.8 m, receiver height is 1.6 m, $\sigma = 2 \times 10^5 \text{ N s m}^{-4}$, and $\alpha = 0.14$. Source-receiver distance is (a) 60 m, (b) 120 m, (c) 200 m, and (d) 400 m.

Parkin and Scholes presented their results at different distances compared to the sound level measured at a reference distance of about 20 m from the source. They also made an estimate of the exact location of the source, in the output stream of a jet engine. To compare our results, we had to carry out the same subtraction. Doing so, we always found a small shift in the interference maxima and minima in the higher frequencies. This is partially due to our different microphone height, but we also assume that the distance in the reference measurements of Parkin and Scholes or the source height was slightly incorrect, probably because the source in a jet stream is not exactly known. The plots used for comparison are Fig. 3 and 4 of Ref. 17, which are not given here. The best agreement is found with the “winter measurements” of Fig. 4. To find good agreement with the “summer plots” of Fig. 3, a lower value of σ must be taken.

The results without wind agree very well in the frequency region from 50–500 Hz. In the region from 630–4000 Hz, we (and many other investigators) find decreasing sound levels with increasing source-receiver distance [see Fig. 11(a)]. Parkin and Scholes found sound levels that no longer decrease for increasing distances. However, Parkin and Scholes measured their no-wind situation when the wind speed was perpendicular to the direction of the sound propagation. Daigle¹⁹ explained the disagreement as due to turbulence and introduced variations in path length between direct and reflected waves around a mean value.

When we compare the results in the downwind situation [as in Fig. 11(b)] with the measurements of Parkin and Scholes, we find surprisingly good agreement over the entire frequency range, except for the dip at 200 Hz for a distance of 400 m. For the upwind case, we again find very good agreement with the measurements in the region up to 500 Hz. Parkin and Scholes, however, found constant sound levels in the frequencies above 500 Hz at about -20 to -25 dB. Our model always finds curves that are steadily decreasing in the shadow region [see Fig. 11(c)]. There are probably other phenomena (vertical wind speeds, scattering at an uneven ground, etc.) causing some high-frequency sound to penetrate into the shadow region in the real situation. These effects are beyond the scope of the present model.

IV. DISCUSSION

The model presented in this paper is a powerful tool for calculating the influence of wind and temperature gradients on sound propagation. It uses a stepwise extrapolation through layers parallel to the ground surface. The mathematics behind the model is based on the full wave equation in the wavenumber domain in three dimensions (k_x , k_y , and z). However, to keep CPU time low, the extrapolation is carried out in two dimensions only. To make a Fourier transform possible from the k_x , z domain to the x , z domain, a transform over the complex wavenumber had to be introduced to avoid a pole in the k_x , z domain.

The resulting propagation equations are relatively simple and, as a consequence, the CPU time within each layer is very short. Therefore, thin layers (if desired on the order of centimeters) can be applied, and any complicated gradient may be introduced.

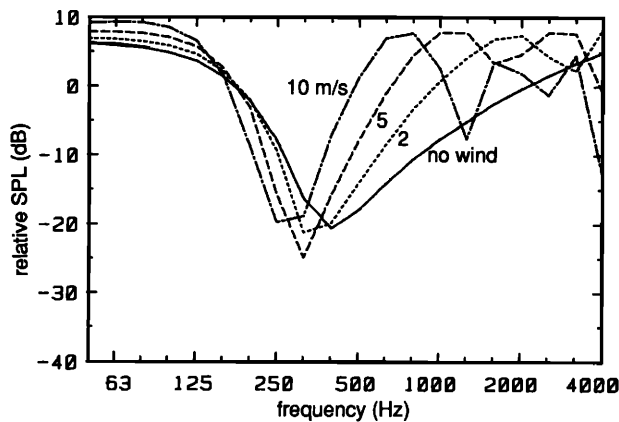


FIG. 7. Frequency plots to illustrate the influence of the wind speed. Source height is 1.8 m, receiver height is 1.6 m, source-receiver distance is 200 m, $\sigma = 2 \times 10^5 \text{ N s m}^{-4}$, and $\alpha = 0.14$.

to the level found in the homogeneous case at the same distance without a ground plane (free-field propagation). The curves are calculated with a flow resistance $\sigma = 2 \times 10^5 \text{ N s m}^{-4}$, for four wind speeds: 0, 2, 5, and 10 m/s. For all of the curves, $\alpha = 0.14$, the source height is 1.8 m, the receiver height is 1.6 m, and the distance from source to receiver is 200 m.

The zero-wind curve is within a few tenths of a dB when compared to the numerous results from calculations and measurements as published in literature for the ground effect. For comparison we used a model developed by Koers,¹⁵ based on the theoretical work of Attenborough *et al.*¹⁶ The results prove to be insensitive to the fact that we use a two-dimensional model.

The curves demonstrate that the sound-pressure level gradually increases with wind speed in the frequency region above 315 Hz. It is interesting to see that the difference between 0 and 2 m/s is larger than between 5 and 10 m/s. There is a tendency (found in other calculations that are not presented in this paper) toward a decrease in sound levels at higher frequencies for a wind speed of 10 m/s.

Figure 8 gives the upwind case. At higher wind speeds, the sound has to penetrate into the shadow region. This appears possible only for the lower frequencies. At a wind speed of -2 m/s , the sound propagation is just above the boundary ray of the shadow zone. As expected, the curve then strongly resembles the curve that is found when the source is at the ground surface in the no-wind situation.

The influence of the source height is shown in Fig. 9. The source height is now 0.5 m. The zero-wind curve shows lower sound levels at higher frequencies. The increase with increasing wind speed from 0–2 m/s is greater than in Fig. 7.

Figure 10 is similar to Fig. 7, but the ground plane is more absorbing ($\sigma = 5 \times 10^4 \text{ N s m}^{-4}$). The decrease in sound level found between 160 and 315 Hz with increasing wind speed in Fig. 7 has now almost completely vanished. Again, we see in Fig. 9 and 10 that the frequency interval is too coarse to give an accurate account of the frequency dips above 500 Hz.

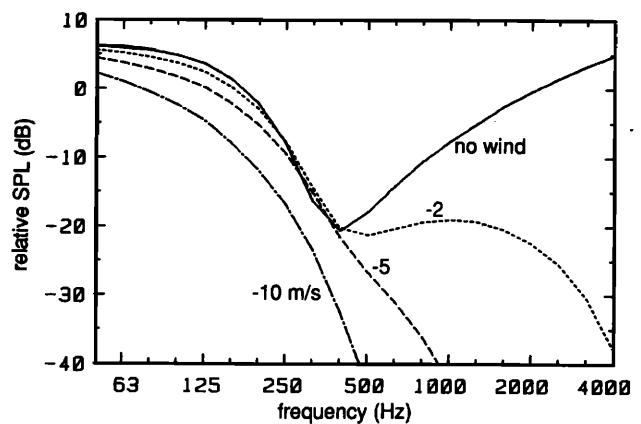


FIG. 8. As in Fig. 7, but for upwind propagation.

E. Frequency plots compared with results from literature

Our initial results from the computer showed a strong resemblance with the results of de Jong, except for the region between 200 and 500 Hz. Introducing a linear temperature profile in our model, we found excellent agreement with the results of Rasmussen [his Fig. 5(a) in Ref. 4]. Because of the limited data available from previous calculation models, a more detailed comparison of our calculations will be made with the outdoor measurements of Parkin and Scholes.^{17,18}

In Fig. 11(a), frequency plots are given for four distances between source and receiver (60, 120, 200, and 400 m) for the homogeneous case. The sound-pressure levels are relative to free-field propagation from a monopole source. Figure 11(b) and (c) gives the results for $+5$ - and -5 -m/s wind speeds. Again, the very deep dip in the frequency curve at 200 Hz can be seen for curve d in Fig. 1(b).

These calculations are used as a basis for comparison with the measurements of Parkin and Scholes. We had to make assumptions about the impedance of the ground surface and wind profile in the measurements. We assumed $\sigma = 2 \times 10^5$ and $\alpha = 0.14$, where the value for the flow resistivity is from de Jong.² Our microphone height was 1.6 m, while Parkin and Scholes gave theirs as 5 ft (1.52 m).

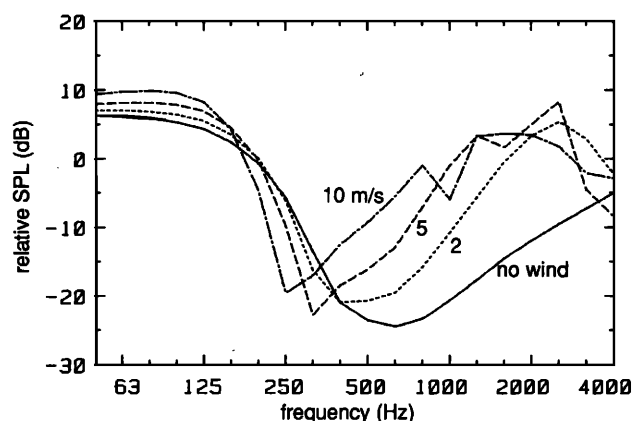


FIG. 9. As in Fig. 7, but with the source at 0.5 m above the ground plane.

The required memory space of the Fourier series in the computer increases with frequency. Applying a zoom-fft appears a useful method for keeping these values constant above 1000 Hz. A complete set of x, z plots (21 frequencies at $12.4 \times 400 \text{ m}^2$) takes about 70 min when the model is run on a vector-based machine. While we deliberately used small layers, no attempt was made to optimize CPU time. This time is very short compared to calculation models based on Bessel-Hankel transforms. Although the model is two dimensional, it is in excellent agreement with numerous previous models for the zero-wind case, which calculate the influence of an absorbing ground surface on sound propagation.

Basically, a wind gradient is a vector, while a temperature gradient is a scalar effect. The model is able to distinguish these effects but, from theoretical considerations and from computer calculations, we found that the differences are small. Because the gradient of the wind speed is much more important than the absolute value of the wind speed (mainly given at 10 m), outdoor measurements of the wind speed should always be carried out at a number of heights, starting as low as possible (for instance, at 0.20 m).

The direct comparison of the results of our model with previous calculations is difficult, because results from previous models in the case of complicated wind profiles are scarce. When a linear temperature profile is introduced in our calculations, a comparison can be made with Rasmussen's model and excellent agreement is found. The agreement with other models is good when compared qualitatively, but varies from fair to poor when looking at the exact numerical results.

A comparison is made with the very extensive measurements of Parkin and Scholes. Very good agreement is found for frequencies below 500 Hz for three cases: downwind, no wind (which is when the wind direction is perpendicular to the sound propagation), and upwind. The agreement for frequencies between 500 and 4000 Hz is only very good in the downwind case.

No agreement is found in the upwind case for frequencies above 500 Hz. Parkin and Scholes found a (low) constant sound level. In our calculations, only low-frequency sound was able to penetrate into the shadow zone.

The only physical restriction of our model was the absence of variations in the propagation parameter in the x direction. To overcome this problem, we want to extend the model in future research. The sound propagation is calculated from the source of a certain x value, assuming constant parameters over that x region. Then, a restart is made at that x value with other parameters, introducing a distribution of source strengths. In that case, we will return to an improved version of the model of de Jong. This model combined x and z extrapolation, and therefore was able to calculate the effects of gradients varying with distance, but could also calculate the influence of sound screens, impedance jumps, etc.

Since there is rapid development in vector-based computers, we will also make an attempt to optimize CPU time and to run the program on a new computer configuration.

ACKNOWLEDGMENTS

The authors wish to thank Rob Witte, who did much initial work on the conversion of the seismic equations to the equations used in outdoor sound propagation. We also want to thank Professor P. M. van den Berg of the Faculty of Electrical Engineering of our university for helpful hints on the Fourier transform with complex variables.

¹B. A. de Jong, "A new method for calculation of the influence of wind and temperature," *Proceedings of the 1980 International Conference on Noise Control Engineering* (INCE, Poughkeepsie, NY, 1980).

²B. A. de Jong, "The influence of wind and temperature gradients on outdoor sound propagation," Ph.D. thesis, Delft University of Technology (1983).

³R. Raspet, S. W. Lee, E. Kuester, D. C. Chang, W. F. Richards, R. Gilbert, and N. Bong, "A fast field program for sound propagation in a layered atmosphere above an impedance ground," *J. Acoust. Soc. Am.* **77**, 345-352 (1985).

⁴K. B. Rasmussen, "Outdoor sound propagation under the influence of wind and temperature gradients," *J. Sound Vib.* **104**, 321-335 (1986).

⁵S. W. Lee, N. Bong, W. F. Richards, and R. Raspet, "Impedance formulation of the fast field program for acoustic wave propagation in the atmosphere," *J. Acoust. Soc. Am.* **79**, 628-634 (1986).

⁶T. L. Richards and K. Attenborough, "Accurate FFT-based Hankel transforms for predictions of outdoor sound propagation," *J. Sound Vib.* **109**, 157-167 (1986).

⁷C. P. A. Wapenaar, "Pre-stack migration in two and three dimensions," Ph.D. thesis, Delft University of Technology (1986).

⁸B. Ursin, "Review of elastic and electromagnetic wave propagation in horizontally layered media," *Geophysics* **48**, 1063-1081 (1983).

⁹D. C. Pridmore-Brown, "Sound propagation in a temperature- and wind-stratified medium," *J. Acoust. Soc. Am.* **34**, 438-443 (1962).

¹⁰H. Kwakernaak and R. Sivan, *Linear Optimal Control Systems* (Wiley, New York, 1972).

¹¹M. E. Delany and E. N. Bazley, "Acoustical properties of fibrous absorbent materials," *Appl. Acoust.* **3**, 105-116 (1970).

¹²A. J. Berkhout, *Seismic Migration, Vol. A, Theoretical Aspects* (North-Holland, Amsterdam, Netherlands, 1982).

¹³W. H. T. Huisman, M. J. Martens, and W. van Asseldonk, "Measured and modelled temperature effects on outdoor sound transmission," *Proc. Inst. Acoust.* **9** (to be published).

¹⁴R. Geiger, *Das Klima der bodennahen Luftschicht* (Vieweg, Braunschweig, Federal Republic of Germany, 1961).

¹⁵P. Koers, "A calculation method for the propagation of outdoor sound over several kinds of barriers on an inhomogeneous ground," M.Sc. thesis, Institute of Applied Physics, Delft, Netherlands (1983).

¹⁶K. Attenborough, S. I. Hayek, and J. M. Lawther, "Propagation of sound above a porous half-space," *J. Acoust. Soc. Am.* **68**, 1493-1501 (1980).

¹⁷P. H. Parkin and W. E. Scholes, "The horizontal propagation of sound from a jet engine close to the ground, at Radlett," *J. Sound Vib.* **1**, 1-13 (1964).

¹⁸P. H. Parkin and W. E. Scholes, "The horizontal propagation of sound from a jet engine close to the ground, at Hatfield," *J. Sound Vib.* **2**, 353-374 (1964).

¹⁹G. A. Daigle, "Effects of atmospheric turbulence on the interference of sound waves above a finite impedance boundary," *J. Acoust. Soc. Am.* **65**, 45-49 (1979).